Sparsening Conformal Arrays Through a Versatile BCS-Based Method

Giacomo Oliveri, *Senior Member, IEEE*, Ephrem T. Bekele, Fabrizio Robol, and Andrea Massa, *Member, IEEE*

***Abstract*—Sparsening conformal arrangements is carried out through a versatile Multi-Task Bayesian Compressive Sensing $(MT-BCS)$ strategy. The problem, formulated in a probabilistic fashion as a pattern-matching synthesis, is that of determining the sparsest excitation set (locations and weights) fitting a reference pattern subject to user-defined geometrical constraints. Results from a set of representative numerical experiments are presented to illustrate the key-features of the proposed approach as well as to assess, also through comparisons, its potentials in terms of matching accuracy, element saving, and computational costs.**

***Index Terms*—Bayesian compressive sampling, conformal arrays, constrained array synthesis, sparse arrays.**

I. Introduction and Motivation

THE problem of designing an array conformal to a non-planar surface [1], [2] arises in several applications [3]–[5] where the layout is severely constrained by aerodynamic requirements as in airborne systems [6] or limitations on the available space as in satellites [7]. However, the synthesis of conformal arrays has proven to be a complex task because, on the one hand, the well-known Fourier transform relationships between element excitations and far field pattern do not hold true [8], and, on the other, this latter depends on each (although identical) element because of its different orientation [7]. Therefore, a wide set of methodologies has been developed [3]–[5], [8]. Concerning *regular* conformal arrangements, several solutions including projection-based methods [3]–[5], [8], [9], iterative least square techniques [10]–[12], adaptive methods [13], linear programming [14], and stochastic optimizers such as simulated annealing [15], particle swarm, and genetic algorithms (GA) [16]–[19] have been proposed to determine the optimal excitations. Nevertheless, few methodologies have been developed so far for synthesizing non-regular layouts [20] even though non-uniform geometrical configurations provide in principle several advantages over regular architectures in terms of weight, consumption, feeding network complexity, computational burden, and costs [20]. Thanks to these features, sparse conformal arrays turn out to be attractive architectural solutions especially when the available power and the payload are heavily limited such as in unmanned aerial vehicles $(UAVs)$ [20]. As for the state-of-the art literature on non-regular conformal design, a GA-based procedure [21] has been recently introduced for designing retrodirective array [20]. Such an approach yields excellent sidelobe level (SLL) control over a wide scan angle [20] thanks to the well-known effectiveness of evolutionary algorithms in solving non-regular array design problems [22], [23], even though it cannot be easily applied to large layouts owing to the arising computational burden and the convergence issues [20], [21].

As far as the efficient synthesis of huge sparse arrangements is concerned, the real-valued linear $(1D)$ case has been dealt with in [24] by means of an innovative Bayesian technique to define the optimal non-regular layout by maximizing the *a-posteriori* distribution probability of the excitations to match a target pattern, while assuming sparseness priors on the element arrangement [24]. The arising Single-Task (ST) Bayesian Compressive Sensing (BCS) formulation [25] has been then efficiently solved through a Relevance Vector Machine (RVM) [26] yielding both the optimal positions and the optimal excitations of the array [24]. Such an approach, which has been also extended to complex-valued-excitations through a Multi-Task (MT) BCS solver [27] as well as to address planar $(2D)$ problems [28], seems to be a good candidate for designing conformal apertures because of the flexibility (i.e., the ability to take into account arbitrary geometrical constraints) and the numerical efficiency in high-dimensional problems [28] proven in other "sparse" electromagnetic problems [29]–[32]. On the other hand, it is worth pointing out that a generalization to the conformal case is not trivial and it needs to be carefully addressed since (a) an improper sampling strategy of the reference pattern leads to an ill-conditioning of the arising transformation kernel and, in turn, a very slow convergence of the RVM solver [28]; (b) a non-ideal choice of the candidate locations for the array elements (i.e., number and displacement over a conformal aperture) does not guarantee a satisfactory trade-off between degrees-of-freedom and computational burden. This is much more critical than in $1D$ and $2D$ cases because of the increased problem dimensionality; (c) unlike $1D$ and $2D$ cases, the element pattern (even though of identical radiators) cannot be neglected during the synthesis process since the radiated pattern is here not simply the product between the element pattern and the array factor, but it also depends on the element orientation [7]. This work is then aimed at formulating and validating a customized BCS-based approach for the design of non-uniform conformal arrangements matching an arbitrary

Manuscript received November 10, 2012; revised September 15, 2013; accepted October 06, 2013. Date of publication October 30, 2013; date of current version April 03, 2014.

The authors are with the ELEDIA Research Center, DISI, University of Trento, Povo 38123 Trento, Italy (e-mail: giacomo.oliveri@disi.unitn.it; bekele,@disi.unitn.it; fabrizio.robol@disi.unitn.it; andrea.massa@unitn.it).

Color versions of one or more of the figures in this paper are available online at http://ieeexplore.ieee.org.

Digital Object Identifier 10.1109/TAP.2013.2287894

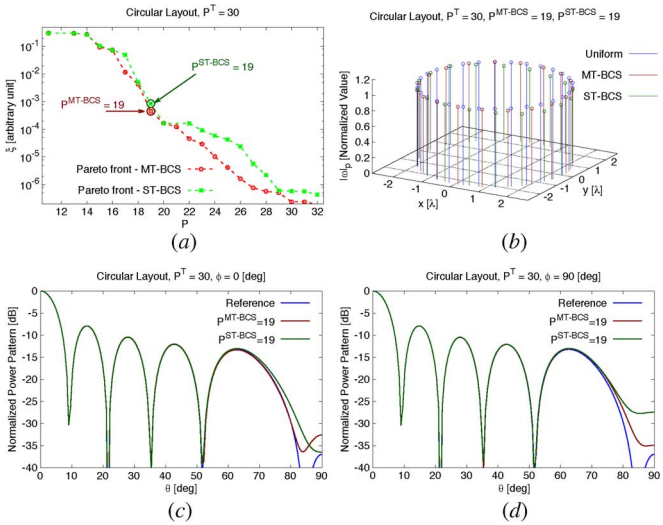

Fig. 1. *Unconstrained synthesis* (*Circular layout*, $P^T = 30$)—Pareto fronts of $MT-BCS$ and $ST-BCS$ solutions in the $(\xi, \widetilde{P})$ plane (a). Synthesized excitation amplitudes (b) and corresponding power patterns at the angular cuts: (c) $\phi = 0$ [deg] and (d) $\phi = 90$ [deg].

reference pattern. Towards this end, the following three main contributions are introduced:

- a generalization of the guidelines in [24], [27], [28] to recast the conformal array synthesis problem into a Bayesian one taking into account the radiation pattern of each array element;
- suitable strategies for sampling the reference pattern and choosing the candidate locations of the array elements to yield satisfactory performances;
- the integration of an array element merging procedure to guarantee a large number of DOFs for the BCS synthesis (i.e., a fine grid for the candidate locations), while enabling the end-user to specify a lower bound for the inter-element spacing of the synthesized layout.

II. Statement of the Synthesis Problem

Let us consider the design of a P-element conformal array whose p-th element is located at $\underline{\rho}_p$ and excited with a weight ω_p, $p = 0, \ldots, P-1$, such that (i) the array element positions belong to an arbitrarily shaped region Υ [Fig. 1(a)], (*ii*) the integral error between the radiated far-field pattern and the target one, $F^T(\theta, \phi)$, in a set of K directions, (θ_k, ϕ_k), $k = 0, \ldots, K-1$, is below a given threshold value ε, and (*iii*) P is minimum. Moreover, let us assume that the P element locations belong to a set of $N \gg P$ user-defined candidate locations at $\underline{r}_n = (x_n, y_n, z_n) \in \Upsilon$ [24], [27]. Each candidate position is associated to an antenna pattern, $E_n(\theta, \phi)$, $n = 0, \ldots, N-1$, modeling the array element radiation which depends on the type of the radiating element as well as on its orientation. Under these hypotheses, the complex-valued design of sparse conformal arrays can be mathematically formulated as follows:

$$\widehat{\underline{w}} = \arg\left\{\min_{\underline{w}} \|\underline{w}\|_{\ell_0}\right\} \text{ subject to } \underline{F}^T - (\mathbf{E} \otimes \mathbf{\Psi})\underline{w} = \underline{d} \quad (1)$$

where $\underline{w} \triangleq \{w_n, n = 0, \ldots, N-1\}$ is the "fictitious" excitation vector of N elements where $w_n \neq 0$ indicates that one of the P element of the sparse array has been placed at the candidate location (x_n, y_n, z_n), $\underline{F}^T \triangleq \{F^T(\theta_k, \phi_k), k = 0, \ldots, K-1\}$ is the target-field column vector[1], $\underline{d}$ is a K-size vector whose k-th entry, d_k, is a zero-mean complex-valued Gaussian variable with variance σ proportional to the pattern matching tolerance ε [24], [27], $\otimes$ stands for the element-wise product

$$\mathbf{E} \triangleq \{e_{kn} = E_n(\theta_k, \phi_k), k = 0, \ldots, K-1, n = 0, \ldots, N-1\} \quad (2)$$

is the element-pattern matrix, and

$$\mathbf{\Psi} \triangleq \{\psi_{kn} = \exp\left[i2\pi \underline{r}(\theta_k, \phi_k) \cdot \underline{r}_n\right], \quad k = 0, \ldots, K-1, n = 0, \ldots, N-1\} \quad (3)$$

is the radiation operator for the conformal case, $\underline{r}(\theta, \phi)$ being the position vector given by [1]

$$\underline{r}(\theta, \phi) \triangleq [\sin(\theta)\cos(\phi), \sin(\theta)\sin(\phi), \cos(\theta)]\,.$$

It is worthwhile to point out that, since the number of non-null entries of $\underline{w}$ is equal to $\|\underline{w}\|_{\ell_0} = \sum_{n=0}^{N-1} |w_n|^0 = P$, the solution of (1) actually identifies the sparsest conformal architecture complying with the requirements (*i*)–(*iii*).

In principle, several deterministic [8], [10] and stochastic [21]–[23] approaches could be used for solving (1). However, a CS technique seems to be a suitable candidate [33] owing to the linearity, ill-conditioning/ill-posedness [24], [27], and sparseness of the problem at hand. Unfortunately, the use of widely-adopted CS algorithms minimizing ℓ_1-based functionals [34] is prevented because of the computationally unfeasible check of the restricted isometry property (RIP)[2] of the problem/transformation kernel, $\mathbf{E} \otimes \mathbf{\Psi}$. Therefore, a BCS perspective is applied hereinafter [24], [27] by rewriting (1) in a probabilistic fashion

$$\widehat{\underline{w}}_Q = \arg\left\{\max_{\underline{w}_Q} \left[\mathcal{P}\left(\underline{w}_Q | \underline{F}_Q^T\right)\right]\right\} \quad (Q = R, I) \quad (4)$$

where $\widehat{\underline{w}}_Q$ is sparse [27] and it satisfies the following relation:

$$\widehat{\underline{w}} = \widehat{\underline{w}}_R + i\widehat{\underline{w}}_I. \quad (5)$$

In (4), $\underline{w}_R \triangleq \mathcal{R}(\underline{w})$, $\underline{w}_I \triangleq \mathcal{I}(\underline{w})$, $\underline{F}_R^T$ and $\underline{F}_I^T$ are the real-valued decomposition of $\underline{F}^T$ such that $\underline{F}_R^T + \underline{F}_I^T = [\mathcal{R}(\underline{F}^T), \mathcal{I}(\underline{F}^T)]'$ and

$$\underline{F}_R^T - \begin{bmatrix}\mathcal{R}(\mathbf{E} \otimes \mathbf{\Psi}) \\ \mathcal{I}(\mathbf{E} \otimes \mathbf{\Psi})\end{bmatrix}\underline{w}_R = \underline{d}_R \quad (6)$$

$$\underline{F}_I^T - \begin{bmatrix}-\mathcal{I}(\mathbf{E} \otimes \mathbf{\Psi}) \\ \mathcal{R}(\mathbf{E} \otimes \mathbf{\Psi})\end{bmatrix}\underline{w}_I = \underline{d}_I \quad (7)$$

where $\underline{d}_R + \underline{d}_I = [\mathcal{R}(\underline{d}), \mathcal{I}(\underline{d})]'$, the subscript $\cdot'$ indicating the transpose operator [27].

[1]In this formulation the target field vector is complex valued (i.e., both its amplitude and its phase are needed to perform the synthesis).

[2]The RIP is a sufficient condition for ℓ_1-norm CS tools to yield accurate estimates [33] of sparse problems. It requires at least $2 \times [(2N)!]/[(2P)!][(2N-2P)!]$ vector norms $[(2N)!]/[(2P)!][(2N-2P)!]$ matrix-vector multiplications for its verification [33].

III. Synthesis Procedure

A. $MT-BCS$ Estimation of the Excitations

Let us notice that both the single-task ($ST-BCS$) and the multi-task ($MT-BCS$) versions of the BCS method have been considered to solve formulations analogous to (4) [24], [27]. However, the $MT-BCS$ technique is the favorite candidate to effectively address the problem at hand since it (a) intrinsically accounts for the *a-priori* knowledge on the sparseness of $\underline{w}_Q (Q=R,I)$, (b) enables a computationally efficient solution, and (c) unlike the $ST-BCS$ case, statistically links the array locations were $\underline{w}_R|_n \neq 0$ and $\underline{w}_I|_n \neq 0$. Accordingly, the generalization of the $MT-BCS$ methodology to the conformal case will be presented hereinafter. More specifically, the $MT-BCS$ posterior probability is firstly considered [27]

$$\mathcal{P}\left(\underline{w}_Q|\underline{F}_Q^T\right) = \int \mathcal{P}\left(\underline{w}_Q|\underline{F}_Q^T,\underline{a}\right)\mathcal{P}\left(\underline{a}|\underline{F}_Q^T\right)d\underline{a} \quad (Q=R,I) \tag{8}$$

where $\underline{a}=\{a_n, n=0,\ldots,N-1\}$ is the *shared hyperparameter* vector that statistically links $\widehat{\underline{w}}_R$ and $\widehat{\underline{w}}_I$. As a matter of fact, a unique $\underline{a}$ independent on Q enables $\mathcal{P}(\underline{w}_Q|\underline{F}_Q^T)$ to account for the relationships between the real and imaginary parts of the unknown array excitations [27].

To made explicit (8), $\mathcal{P}(\underline{w}_Q|\underline{F}_Q^T,\underline{a})$ and $\mathcal{P}(\underline{a}|\underline{F}_Q^T)$ need to be specified. As for the former, the approach discussed in [27] can be generalized to deduce the following multivariate *Student-t* distribution [35]

$$\mathcal{P}\left(\underline{w}_Q|\underline{F}_Q^T,\underline{a}\right) = \left(\int_0^\infty \kappa^{\gamma_1+\frac{N}{2}-1}e^{-\kappa}\mathrm{d}\kappa\right)^{-1} \times \frac{\left[1+\frac{(\underline{w}_Q-\underline{\mu}_Q)'Z_Q^{-1}(\underline{w}_Q-\underline{\mu}_Q)}{2\gamma_2}\right]^{-\left(\gamma_1+\frac{N}{2}\right)}}{\left(\int_0^\infty \kappa^{\gamma_1-1}e^{-\kappa}\mathrm{d}\kappa\right)(2\pi\gamma_2)^{\frac{N}{2}}\sqrt{|G_Q|}} \quad (Q=R,I) \tag{9}$$

where

$$\begin{cases} \underline{\mu}_R \triangleq \mathbf{G}_R^{-1}\left[\mathcal{R}(\mathbf{E}\otimes\mathbf{\Psi}),\mathcal{I}(\mathbf{E}\otimes\mathbf{\Psi})\right]\underline{F}_R^T \\ \underline{\mu}_I \triangleq \mathbf{G}_I^{-1}\left[-\mathcal{I}(\mathbf{E}\otimes\mathbf{\Psi}),\mathcal{R}(\mathbf{E}\otimes\mathbf{\Psi})\right]\underline{F}_I^T \end{cases} \tag{10}$$

and

$$\begin{cases} \mathbf{G}_R \triangleq diag(\underline{a}) + \left[\mathcal{R}(\mathbf{E}\otimes\mathbf{\Psi}),\mathcal{I}(\mathbf{E}\otimes\mathbf{\Psi})\right] \\ \quad \cdot\left[\mathcal{R}(\mathbf{E}\otimes\mathbf{\Psi}),\mathcal{I}(\mathbf{E}\otimes\mathbf{\Psi})\right]' \\ \mathbf{G}_I \triangleq diag(\underline{a}) + \left[-\mathcal{I}(\mathbf{E}\otimes\mathbf{\Psi}),\mathcal{R}(\mathbf{E}\otimes\mathbf{\Psi})\right] \\ \quad \cdot\left[-\mathcal{I}(\mathbf{E}\otimes\mathbf{\Psi}),\mathcal{R}(\mathbf{E}\otimes\mathbf{\Psi})\right]'. \end{cases} \tag{11}$$

As for the other term within the integral on the right-hand side of (8), a "delta-function" approximation is adopted since a closed-form expression is not available [35]

$$\mathcal{P}\left(\underline{a}|\underline{F}_Q^T\right) \approx \delta(\underline{a}-\widehat{\underline{a}}) \tag{12}$$

where $\widehat{\underline{a}}$ is the hyperparameter posterior *mode* computed as $\widehat{\underline{a}} = \arg\{\max_{\underline{a}}[\mathcal{L}(\underline{a})]\}$ being [35]

$$\mathcal{L}(\underline{a}) = -\frac{1}{2}\log\left\{|\mathbf{B}_R||\mathbf{B}_I|\left[\left(\left(\underline{F}_R^T\right)'\mathbf{B}_R^{-1}\underline{F}_R^T+2\beta_2\right)\times\left(\left(\underline{F}_I^T\right)'\mathbf{B}_I^{-1}\underline{F}_I^T+2\beta_2\right)\right]^{(N+2\beta_1)}\right\} \tag{13}$$

is the logarithm of the $MT-BCS$ "marginal likelihood" and

$$\begin{cases} \mathbf{B}_R \triangleq \mathbf{I} + \left[\mathcal{R}(\mathbf{E}\otimes\mathbf{\Psi}),\mathcal{I}(\mathbf{E}\otimes\mathbf{\Psi})\right]'diag(\underline{a})^{-1} \\ \quad \cdot\left[\mathcal{R}(\mathbf{E}\otimes\mathbf{\Psi}),\mathcal{I}(\mathbf{E}\otimes\mathbf{\Psi})\right] \\ \mathbf{B}_I \triangleq \mathbf{I} + \left[-\mathcal{I}(\mathbf{E}\otimes\mathbf{\Psi}),\mathcal{R}(\mathbf{E}\otimes\mathbf{\Psi})\right]'diag(\underline{a})^{-1} \\ \quad \cdot\left[-\mathcal{I}(\mathbf{E}\otimes\mathbf{\Psi}),\mathcal{R}(\mathbf{E}\otimes\mathbf{\Psi})\right] \end{cases}$$

$\mathbf{I}$ being the N-size identity matrix. Likewise the $ST-BCS$, the maximization of (13) is then carried out by means of an efficient RVM solver [35], [37].

By substituting (9) and (12) in (8), the solution of (4) is

$$\widehat{\underline{w}}_Q = \arg\left\{\max_{\underline{w}_Q}\left[\mathcal{P}\left(\underline{w}_Q|\underline{F}_Q^T,\underline{a}\right)\big|_{\underline{a}=\widehat{\underline{a}}}\right]\right\} = \underline{\mu}_Q\big|_{\underline{a}=\widehat{\underline{a}}} \tag{14}$$

since the *mode* of a multi-variate *Student-t* distribution is equal to its *average* value [i.e., $\underline{\mu}_Q$ in (10)]. Finally, the excitation vector (5) turns out to be equal to

$$\begin{aligned} \widehat{\underline{w}} = {} & \left[diag(\widehat{\underline{a}}) + \left[\mathcal{R}(\mathbf{E}\otimes\mathbf{\Psi}),\mathcal{I}(\mathbf{E}\otimes\mathbf{\Psi})\right]\right. \\ & \left.\times\left[\mathcal{R}(\mathbf{E}\otimes\mathbf{\Psi}),\mathcal{I}(\mathbf{E}\otimes\mathbf{\Psi})\right]'\right]^{-1} \\ & \times\left[\mathcal{R}(\mathbf{E}\otimes\mathbf{\Psi}),\mathcal{I}(\mathbf{E}\otimes\mathbf{\Psi})\right]\underline{F}_R^T \\ & + i\left[diag(\widehat{\underline{a}}) + \left[-\mathcal{I}(\mathbf{E}\otimes\mathbf{\Psi}),\mathcal{R}(\mathbf{E}\otimes\mathbf{\Psi})\right]\right. \\ & \left.\times\left[-\mathcal{I}(\mathbf{E}\otimes\mathbf{\Psi}),\mathcal{R}(\mathbf{E}\otimes\mathbf{\Psi})\right]'\right]^{-1} \\ & \times\left[-\mathcal{I}(\mathbf{E}\otimes\mathbf{\Psi}),\mathcal{R}(\mathbf{E}\otimes\mathbf{\Psi})\right]\underline{F}_I^T \end{aligned} \tag{15}$$

It must be remarked that the main theoretical difficulty (and innovative contribution) in the derivation of (15) is represented by the decomposition of the complex synthesis problem into two real-valued correlated ones [(6), (7)]. Once the reformulation is at hand, the main numerical challenge is represented by the maximization of (13), but this can be readily performed by RVM solvers available online [35], [37].

B. Element Merging Procedure

Equation (15) represents the generalization of the method presented in [27], [28] to the conformal synthesis problem and, therefore, it could be directly applied to deduce the sparse layout as follows [27]: (a) set $p=0$, $n=0$; (b) if $\widehat{w}_n \neq 0$, set $\widehat{\omega}_p = \widehat{w}_n$, $\underline{\widehat{\rho}}_p = \underline{r}_n$, and update $p \leftarrow p+1$; (c) if $n=N-1$, set $\widehat{P}=p$ and return $(\widehat{\omega}_p, \underline{\widehat{\rho}}_p)$, $p=1,\ldots,\widehat{P}$; otherwise update $n \leftarrow n+1$ and goto (b).

However, such a procedure presents a limitation. Indeed, a large N (i.e., a sufficient number of DoFs) is required to enable optimal performances, but if a very fine grid $\underline{r}_n$ ($n=0,\ldots,N-1$) over Υ is considered, extremely close locations (e.g., $\|\underline{\widehat{\rho}}_p - \underline{\widehat{\rho}}_{p+1}\| \ll \lambda$) can be chosen resulting in practically unfeasible layouts. On the other hand, reducing N to *a-priori* guarantee that the elements are sufficiently far one from the other is not effective since the synthesized layouts turn out sub-optimal.

In order to overcome such a limitation while allowing a sufficient number of DoFs to be used during the design process, an additional post-processing step aimed at merging closely spaced elements is introduced. More specifically, a user-defined minimum element spacing Δ (in wavelength) is defined, and the following procedure is applied:

1) **Initialization**—Set $p=1$, $\widetilde{\omega}_0 = \widehat{\omega}_0$, $\underline{\widetilde{\rho}}_0 = \underline{\widehat{\rho}}_0$, $\widetilde{P}=1$;

2) **Merging**—Scan $q = 0, \ldots, p-1$, if $\exists q$ such that $\Delta_{pq} \triangleq \|\widehat{\underline{\rho}}_p - \widetilde{\underline{\rho}}_q\| \leq \Delta$ then $\widetilde{\underline{\rho}}_q \leftarrow (\widehat{\omega}_p\widehat{\underline{\rho}}_p + \widetilde{\omega}_q\widetilde{\underline{\rho}}_q/\widehat{\omega}_p + \widetilde{\omega}_q)$, $\widetilde{\omega}_q \leftarrow (\widehat{\omega}_p\widehat{\underline{\rho}}_p + \widetilde{\omega}_q\widetilde{\underline{\rho}}_q/\widehat{\omega}_p + \widetilde{\omega}_q)(\widetilde{\omega}_q - \widehat{\omega}_p/\widetilde{\underline{\rho}}_q - \widehat{\underline{\rho}}_p) + [\widehat{\omega}_p - \widehat{\underline{\rho}}_p(\widetilde{\omega}_q - \widehat{\omega}_p/\widetilde{\underline{\rho}}_q - \widehat{\underline{\rho}}_p)]$. Otherwise, $\widetilde{\omega}_{\widetilde{P}} = \widehat{\omega}_p$, $\widetilde{\underline{\rho}}_{\widetilde{P}} = \widehat{\underline{\rho}}_p$ and update $\widetilde{P} = \widetilde{P} + 1$;
3) **Return**—If $p = \widehat{P} - 1$ and $\Delta_{pq} \geq \Delta \forall p, q(p \neq q)$ then return the filtered layout $(\widetilde{\omega}_p, \widetilde{\underline{\rho}}_p; p = 0, \ldots, \widetilde{P} - 1)$ and stop. Otherwise, if $p = \widehat{P} - 1$ then reset $p(p \leftarrow 0)$, else $p \leftarrow p + 1$. Goto 2.

Accordingly, the layout $(\widetilde{\omega}_p, \widetilde{\underline{\rho}}_p)$ after the merging procedure will comprise $\widetilde{P} \leq \widehat{P}$ elements with minimum spacing above Δ.

IV. Numerical Results

This section is aimed at the assessment of the features and performances of the BCS-based conformal array synthesis when dealing with different geometries, apertures, and target patterns. Towards those purposes, the following indexes are analyzed besides the pictorial results concerned with radiation patterns and synthesized layouts: the *element saving ratio*, $\nu \triangleq (\widetilde{P}/P^T)$, P^T being the number of array elements of a uniform layout synthesizing the reference pattern $F^T(\theta, \phi)$, the minimum $(\Delta_{\min})$, the maximum $(\Delta_{\max})$, the average (Δ_{ave}) inter-element spacing of the sparse layout, and the pattern matching accuracy index, ξ, defined as

$$\xi \triangleq \frac{\int_0^{2\pi}\int_0^{\pi}\left|F^T(\theta,\phi) - F(\theta,\phi)\right|^2 d\theta d\phi}{\int_0^{2\pi}\int_0^{\pi}\left|F^T(\theta,\phi)\right|^2 d\theta d\phi}. \tag{16}$$

that quantifies the mismatch between the synthesized pattern and the reference one. Moreover, the control parameters of the $MT-BCS$-based synthesis approach have been chosen according to a calibration procedure similar to those carried out in [27], [28] obtaining the following tradeoff ranges: (a) $N \in [20 \times P^T, 40 \times P^T]$, (b) $K \in [2 \times P^T, 3 \times P^T]$, (c) $\beta_1 \in [10^{-2}, 3\times10^{-2}]$, (d) $\beta_2 \in [0.9, 1]$, and (e) $\sigma \in [5\times10^{-4}, 10^{-3}]$. For the sake of completeness, the $MT-BCS$ results will be compared to those from the generalization of the $ST-BCS$ method [24], [27] to (4), as well as to other state-of-the-art techniques.

A. Unconstrained Synthesis

The first test case of the numerical assessment of the $MT-BCS$ conformal synthesis is concerned with a target pattern afforded by a $P^T = 30$ uniformly-fed $\lambda/2$-spaced circular arrangement with radius $\mu = 15/2\pi$ $[\lambda]$ [Fig. 1(b)]. The array surface Υ has been sampled as follows

$$\begin{cases} x_n = \mu\cos\left(\frac{2\pi n}{N}\right) \\ y_n = \mu\sin\left(\frac{2\pi n}{N}\right) \\ z_n = 0 \end{cases} \quad n = 0, \ldots, N-1 \tag{17}$$

TABLE I
Unconstrained Synthesis (*Circular Layout*, $P^T = 30$)—Performance Indexes

	Reference	$ST-BCS$	$MT-BCS$
P	30	19	10
ξ	-	8.52×10^{-4}	4.50×10^{-4}
ν	1	0.63	0.63
$\Delta_{\min}/\frac{\lambda}{2}$	0.998	1.494	1.521
$\Delta_{\max}/\frac{\lambda}{2}$	0.998	1.612	1.602
$\Delta_{\text{ave}}/\frac{\lambda}{2}$	0.998	1.553	1.565
Δt [s]	–	1.14	4.18

and isotropic radiators have been assumed [i.e., $E_n(\theta, \phi) = 1$]. Moreover, the following uniform pattern sampling strategy has been adopted

$$\begin{cases} \theta_k = \pi\frac{(k \bmod K_\theta)}{K_\theta - 1} \\ \phi_k = 2\pi\frac{\left\lfloor \frac{k}{K_\theta} \right\rfloor}{K_\phi - 1} \end{cases} \quad k = 0, \ldots, K-1 \tag{18}$$

K_ϕ and K_θ complying with $K_\phi \times K_\theta = K$ [28]. The synthesis results are provided in terms of $ST-BCS$ and $MT-BCS$ Pareto fronts in the $(\widetilde{P}, \xi)$ plane [Fig. 1(a)]. As it can be inferred, the two approaches yield closer results whatever the value of $\widetilde{P}$, even though the MT arrangement has a better matching index for a given array size [e.g., $\xi^{MT-BCS}\rfloor_{\widetilde{P}=25} \approx 4.1 \times 10^{-6}$ vs. $\xi^{ST-BCS}\rfloor_{\widetilde{P}=25} \approx 4.3 \times 10^{-5}$—Fig. 1(a)]. The closeness of the performances of the two approaches is even more evident when analyzing the optimal trade-offs [i.e., $\xi^{MT-BCS}\rfloor_{\widetilde{P}=19} \approx 4.5 \times 10^{-4}$ vs. $\xi^{ST-BCS}\rfloor_{\widetilde{P}=19} \approx 8.5 \times 10^{-4}$—Fig. 1(a) and Table I].[3] Indeed, both techniques yield the same element saving factor [$\nu \approx 0.63$—Fig. 1(b)], similar layout features (Table I) as well as close patterns [Figs. 1(c)–1(d)]. Such an outcome is not surprising because of the symmetric and "simple" (i.e., no shaped sidelobes) shape of the target pattern at hand [Figs. 1(c)–1(d)]. It is also confirmed ($\xi^{ST-BCS} < 8.52 \times 10^{-4} \approx \xi^{MT-BCS} < 8.53 \times 10^{-4}$) by varying the array radius within the range $\mu \in [(15/2\pi), (50/\pi)]$ (i.e., $P^T \in [30, 200]$) [Fig. 2]. As for the array sparseness, it decreases when the aperture widens whatever the synthesis approach [e.g., $\nu^{MT-BCS}\rfloor_{P^T=30} \approx 0.63$ vs. $\nu^{MT-BCS}\rfloor_{P^T=150} \approx 0.72$—Fig. 2] because of the increasing problem complexity. However, the behavior of ν shows that the $MT-BCS$ algorithm always yields sparser layouts whatever the reference uniform array [e.g., $\nu^{MT-BCS}\rfloor_{P^T=200} = 0.82$ vs. $\nu^{ST-BCS}\rfloor_{P^T=200} = 0.98$—Fig. 2]. This points out the enhanced effectiveness of the MT implementation when dealing with large arrays radiating even symmetric target patterns [Fig. 2] unlike the $1D$ case where the advantages were slight [27].

To extend the assessment analysis beyond the case Υ lying on the $\theta = 0$ plane [Figs. 1–2], as well as to compare the $MT-BCS$ performance with those of a state-of-the-art

[3]A value of the matching error of about $\xi \approx 10^{-3}$ (obtained by a calibration procedure analogous to those presented in [27], [28]) has been considered throughout the paper to select the $MT-BCS$ trade-off design.

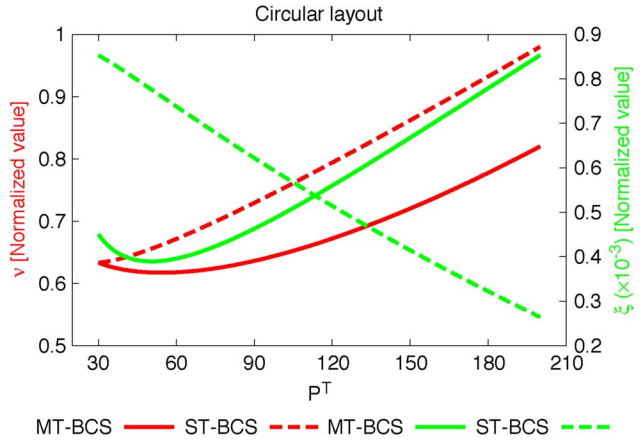

Fig. 2. *Unconstrained synthesis* (*Circular layout*, $P^T \in [20, 200]$)—Plots of ν and ξ versus P^T.

technique, an arrangement conformal to a hemispherical sector [Figs. 3(b)–3(d)] radiating a symmetric beam [Fig. 3(a)] [38] has been considered next. More specifically, the target pattern is related to a non-uniform $P^T = 28$ array [38] displaced over 7 rings laying on an hemisphere of radius $\mu = 2.72$ $[\lambda]$. The pattern has been sampled according to (18) and the following discretization has been used

$$\begin{cases} x_n = \mu \sin\left[\frac{\pi(n \bmod N_\theta)}{2(N_\theta - 1)}\right] \cos\left[2\pi \frac{\left\lfloor \frac{n}{N_\theta} \right\rfloor}{N_\phi - 1}\right] \\ y_n = \mu \sin\left[\frac{\pi(n \bmod N_\theta)}{2(N_\theta - 1)}\right] \sin\left[2\pi \frac{\left\lfloor \frac{n}{N_\theta} \right\rfloor}{N_\phi - 1}\right] \\ z_n = \mu \cos\left[2\pi \frac{\left\lfloor \frac{n}{N_\theta} \right\rfloor}{N_\phi - 1}\right] \end{cases} \quad n = 0, \ldots, N-1 \tag{19}$$

where $N_\theta \times N_\phi = N$. Moreover, the element pattern has been modeled through the following relationship [38]

$$\begin{aligned} E_n(\theta, \phi) &= \left(\sin(\phi) \sin\left[\arctan\left(\frac{y_n}{x_n}\right)\right] + \cos(\phi) \cos\left[\arctan\left(\frac{y_n}{x_n}\right)\right] \right) \\ &\quad \times \exp\left(i 2\pi\mu \left[\cos\theta \cos\left[\arccos\left(\frac{z_n}{\mu}\right)\right] \right.\right. \\ &\quad + \sin\theta \sin\left[\arccos\left(\frac{z_n}{\mu}\right)\right] \\ &\quad \left.\left. \times \cos\left(\phi - \left[\arctan\left(\frac{y_n}{x_n}\right)\right]\right)\right]\right) \end{aligned} \tag{20}$$

The comparison reported in Fig. 3(a) clearly assesses that the MT algorithm outperforms the analytical technique presented in [38] in synthesizing conformal arrangements. More in detail, the $MT - BCS$ optimal trade-off guarantees a high matching accuracy [e.g., $\xi^{MT-BCS} \approx 5.1 \times 10^{-6}$—Fig. 3(a)] with a significantly reduced number of elements, as it is evident when observing the reference [$P^T = 28$—Fig. 3(b), Fig. 3(d)] and synthesized [$\widetilde{P}^{MT-BCS} = 18$—Fig. 3(c), Fig. 3(e)] layouts.

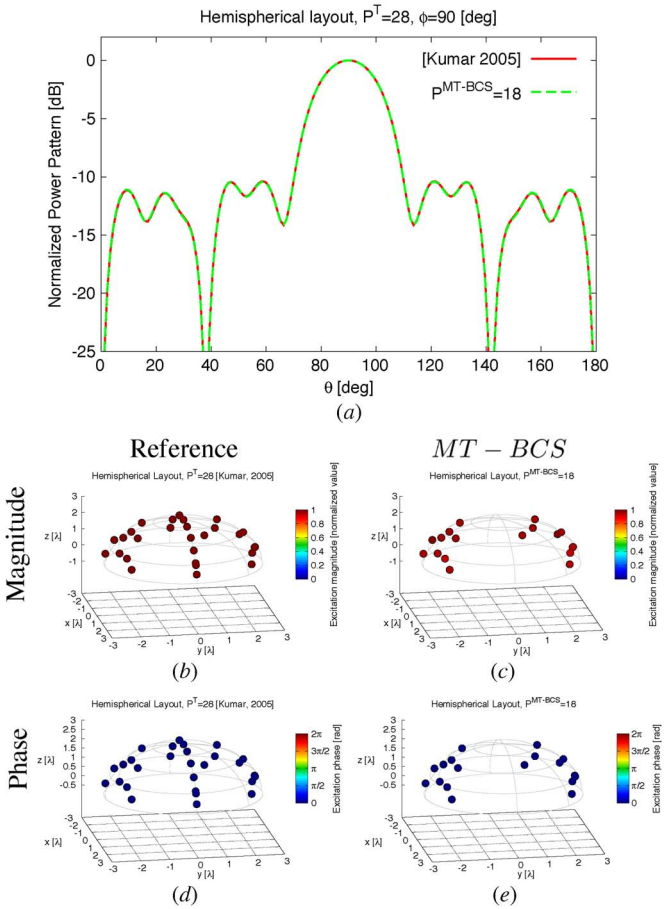

Fig. 3. *Unconstrained synthesis* (*Hemispherical layout*, $P^T = 28$)—Power pattern of reference [38] and tradeoff $MT - BCS$ solution at the angular plane $\phi = 90$ [deg] (a), and reference (b)(d) and $MT - BCS$ (c)(d) excitations [magnitude (b)(c) and phase (d)(e)].

Such a result confirm the effectiveness of the proposed methodology with respect to state-of-the-art synthesis techniques for non-uniform conformal architectures.

B. Aperture-Constrained Synthesis

The previous section has assessed the $MT - BCS$ strategy when dealing with both symmetric and non-symmetric/shaped reference patterns and its advantages/drawbacks over the standard $ST - BCS$ strategy and state-of-the-art methods. On the other hand, it has been shown in [27], [28] that BCS-based approaches have the unique capability to efficiently enforce "forbidden regions" for the array elements thus enabling *aperture constrained* synthesis by means of a simple choice of the candidate locations (x_n, y_n, z_n), $n = 0, \ldots, N-1$. To investigate on such a key feature also in non-uniform conformal arrays, a cylindrical layout (Fig. 4) radiating a shaped beam (Fig. 6) taken from [15] has been analyzed either in the "Unconstrained" case or setting a single forbidden region of size $\lambda \times \lambda$ at the center of the aperture to model a blockage constraint ["Single-Hole"—Fig. 5(c)]. More specifically, the target pattern is related to a $P^T = 64$ array [15] displaced over a $2\pi/9$-wide sector of a cylinder with radius $\mu = 5.0$ $[\lambda]$ and height $h = 3.5$ $[\lambda]$. In the "Unconstrained" case (Table II), the pattern sampling strategy

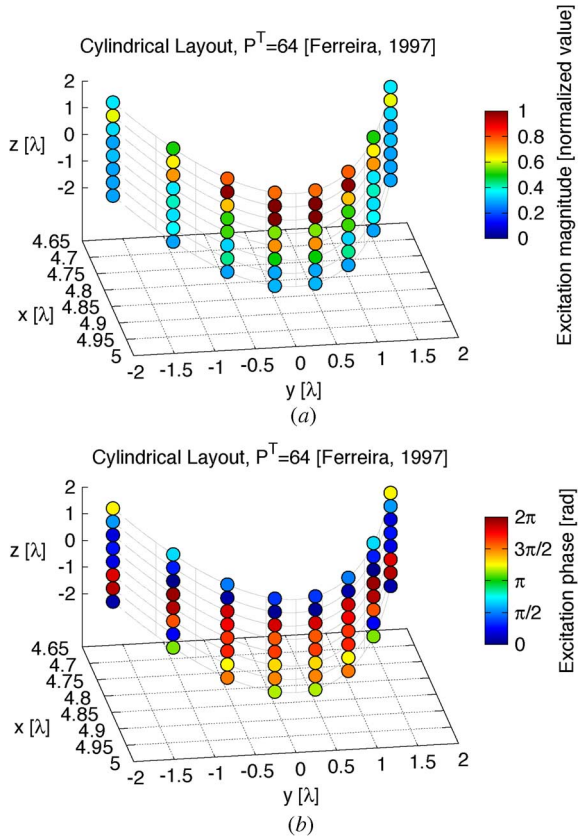

Fig. 4. *Aperture-constrained synthesis* (*Cylindrical layout*, $P^T = 64$ [15])—Reference excitations [amplitude (a) and phase (b)].

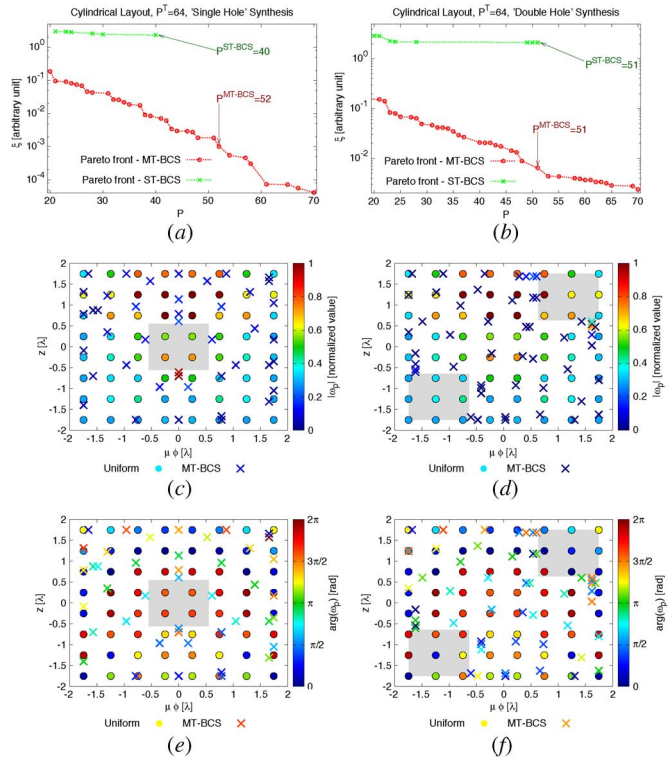

Fig. 5. *Aperture-constrained synthesis* (*Cylindrical layout*, $P^T = 64$ [15])—Pareto fronts of $MT-BCS$ and $ST-BCS$ solutions in the $(\xi, \widetilde{P})$ plane (a)(b). $ST-BCS$ and $MT-BCS$ excitations [amplitude (c)(d) and phase (e)(f)] for (a)(c)(e) the "single hole" and (b)(d)(e) "double hole" geometries.

(18) has been adopted and array aperture has been discretized as follows

$$\begin{cases} x_n = \mu \cos\left[-\frac{\pi}{9} + \frac{2\pi(n \bmod N_\rho)}{9(N_\rho - 1)}\right] \\ y_n = \mu \sin\left[-\frac{\pi}{9} + \frac{2\pi(n \bmod N_\rho)}{9(N_\rho - 1)}\right] \\ z_n = -\frac{h}{2} + h\left(\frac{\lfloor \frac{n}{N_z} \rfloor}{N_z - 1}\right) \end{cases} \quad n = 0, \ldots, N-1 \quad (21)$$

being $N_\rho \times N_z = N$, while the following element pattern has been assumed [15]:

$$E_n(\theta, \phi) = \sin\theta \cos\left[\theta, \phi - \arctan\left(\frac{y_n}{x_n}\right)\right]. \quad (22)$$

As expected, the introduction of a constraint causes the increment of $\widetilde{P}$ for matching the target pattern with a given accuracy [e.g., $\widetilde{P}^{MT-BCS}\big|_{\xi \approx 10^{-3}} = 52$ (constrained aperture) vs. $\widetilde{P}^{MT-BCS}\big|_{\xi \approx 10^{-3}} = 50$ (unconstrained)—Table II]. Despite the higher complexity, the $MT-BCS$ still finds a satisfactory trade-off arrangement ($\widetilde{P}^{MT-BCS} = 52 < P^T$—Table II) complying with the aperture constraints [Fig. 5(c) and Fig. 5(e)] with an acceptable degree of accuracy [i.e., $\xi^{MT-BCS} \approx 10^{-3}$—Fig. 5(a)] as also confirmed by the plots of the associated pattern along two representative cuts [Fig. 6(a)—$\phi = 0$ [deg] and Fig. 5(c)—$\theta = 90$ [deg]]. On the contrary, the $ST-BCS$ pattern does not faithfully reproduce the reference one [i.e., $\xi^{ST-BCS} > 2.0$—Fig. 5(a)].

Similar conclusions can be drawn for multiple or extended "forbidden regions". With reference to the synthesis of the same cylindrical layout of [15] with two blocked areas of size $\lambda \times \lambda$ [Fig. 5(d)], it turns out that the $MT-BCS$ technique outperforms the $ST-BCS$ one in terms of matching error for a given array size [Fig. 6(b) and Fig. 6(d)], or, conversely, number of array elements to reach a given fidelity [Fig. 5(b)]. Of course, the effectiveness of the $MT-BCS$ in achieving satisfactory results is related to the sizes and the locations of the "forbidden regions". Indeed, enforcing the "Two-Holes" constraint (blocking above 16% of the original aperture) does not enable the $MT-BCS$ to meet the $\xi \approx 10^{-3}$ target matching with a sparse (i.e., $\widetilde{P} < P^T$) layout [Fig. 5(b)]. Nevertheless, the plots of the pattern [Fig. 6(b) and Fig. 6(d)] and the layouts [Fig. 5(d) and Fig. 5(f)] of the $MT-BCS$ non-dominated solutions with $\widetilde{P} = 51$ [$\xi \approx 6.4 \times 10^{-3}$—Table II] indicate that non-regular conformal solutions complying with the aperture constraints and giving an accurate reproduction of the reference mainbeam with only some minor mismatching in low sidelobes [Fig. 6(b) and Fig. 6(d)] can still be obtained. The opposite holds true for the $ST-BCS$ generalization [Fig. 5(b)].

C. Spacing-Constrained Synthesis

In order to prevent the final layout has array elements closer than a minimum user-defined distance Δ or to further

TABLE II
Aperture-Constrained Synthesis (*Cylindrical Layout*, $P^T = 64$ [15])—PERFORMANCE INDEXES

		Unconstrained		*"Single-Hole"*		*"Double-Hole"*	
	Ref.	*ST*	*MT*	*ST*	*MT*	*ST*	*MT*
P	64	56	50	40	52	51	51
ξ	–	1.25	7.01×10^{-4}	2.33	1.0×10^{-3}	2.12	6.4×10^{-3}
ν	1.0	0.875	0.781	0.625	0.812	0.797	0.797
$\Delta_{\min}/\frac{\lambda}{2}$	0.997	0.088	0.106	0.499	0.127	0.698	0.127
$\Delta_{\max}/\frac{\lambda}{2}$	0.997	1.186	1.293	1.115	1.401	0.989	1.351
$\Delta_{ave}/\frac{\lambda}{2}$	0.997	0.507	0.810	0.701	0.715	0.721	0.576
Δt [s]	–	9.85	26.77	4.90	37.06	4.65	25.20

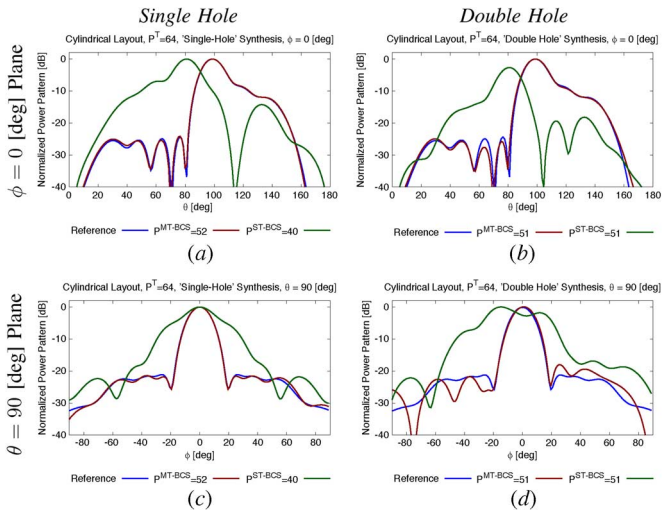

Fig. 6. *Aperture-constrained synthesis* (*Cylindrical layout*, $P^T = 64$ [15])—Power patterns at the angular planes (a) $\phi = 0$ and (b) $\theta = 90$ [deg] in correspondence with (a)(c) the "single hole" and (b)(d) the "double hole" geometries.

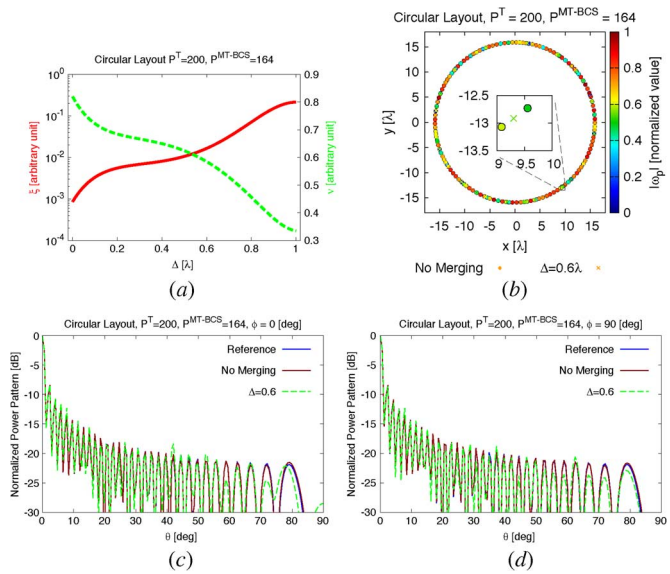

Fig. 7. *Spacing-constrained synthesis* (*Circular layout*, $P^T = 200$)—Plots of ξ and ν versus Δ (a). Excitations (b) and power patterns at the angular cuts $\phi = 0$ [deg] (b) and $\phi = 90$ [deg].

thin the array arrangement, the merging procedure discussed in Section III-B gives a further degree-of-freedom to the antenna designer. This will be made clearer through the following examples by describing the behavior of ν and ξ versus the user-required minimum inter-element distance, Δ. The first test case deals with the circular $MT - BCS$ arrangement comprising $\widehat{P} = 164$ elements synthesized in Section IV-A starting from the $P^T = 200$ uniformly-fed circular layout considered in Fig. 2. As expected, the value of the matching error monotonically increases with Δ [e.g., $\xi|_{\Delta=0} = 8.53 \times 10^{-4}$ vs. $\xi|_{\Delta=0.9\lambda} = 2.08 \times 10^{-1}$—Fig. 7(a)], while the sparseness of the array structure enhances. In order to give some insights on the arising effects, let us analyze the solution at $\Delta = 0.6\lambda$ ["Optimal Merged"—Figs. 7(b)–7(d); Table III]. The synthesized layout turns out to be simplified [e.g., see the inset in Fig. 7(b)] with a further reduction of the array elements with respect to the optimal sparse arrangement ("Optimal"—Table III) [i.e., $\nu|_{\Delta=0} = 0.82$ vs. $\nu|_{\Delta=0.6\lambda} = 0.6$—Fig. 7(a)], while the matching deterioration $[(\xi|_{\Delta=0.6\lambda}/\xi|_{\Delta=0}) \approx 14.8$—Table III] does not dramatically perturb the radiated pattern [Figs. 7(c)–7(d)]. In order to point out the role of the merging procedure, it is also worth noting that the same results in terms of array architecture could not be yielded by just picking from the Pareto front a solution with a matching error close to that of the "Optimal Merged" layout (i.e., $\xi \approx 10^{-2}$—Table III). As a matter of fact, this latter choice ("Sub-optimal", $\xi = 1.82 \times 10^{-2}$—Table III) will guarantee the final arrangement neither to comply with the minimum spacing constraint (i.e., $\Delta_{\min} \approx 0.056$ [λ]—Table III) nor to have the same element saving ($\nu = 0.64$—Table III).

TABLE III
Spacing-Constrained Synthesis (*Circular Layout*, $P^T = 200$)—PERFORMANCE INDEXES

		$MT - BCS$		
	Ref.	Optimal	Optimal Merged	Sub-Optimal
Δ [λ]	–	0.0	0.6	0.0
P	200	164	120	128
ξ	–	8.53×10^{-4}	1.27×10^{-2}	1.82×10^{-2}
ν	1	0.82	0.6	0.64
$\Delta_{\min}/\frac{\lambda}{2}$	1	0.167	1.225	0.111
$\Delta_{\max}/\frac{\lambda}{2}$	1	1.833	1.975	2.000
$\Delta_{ave}/\frac{\lambda}{2}$	1	0.920	1.598	1.246
Δt [s]	–	9.96	9.96	19.65

D. Computational Time

Finally, as far as the computational point of view is concerned, the CPU time, Δt, of the synthesis is re-

ported in Tables I–III when considering the SW implementation of non-optimized Matlab codes running on a single-core desktop PC working at 2.6 GHz. As it can be noticed, the synthesis time grows as the complexity of the problem increases [e.g., $\Delta t\rfloor_{circular} = 4.18$ [s] (Table I) vs. $\Delta t\rfloor_{cylindrical} = 26.7$ [s] (Table II)]. Moreover, and as expected [27], [28], the $MT-BCS$ synthesis is usually more expensive than the $ST-BCS$ (e.g., $\Delta t\rfloor_{MT-BCS}/\Delta t\rfloor_{ST-BCS} \approx 3.66$—Table I). It must be pointed out that such increase is mainly related to the more complicated functional that the RVM has to solve in the MT case [see (13)] with respect to the ST one [24]. However, the overall $MT-BCS$ synthesis often requires less than half a minute, and it does never exceed ≈40 [s] despite the non-optimized nature of the implementation (Tables I–III).

V. Conclusions

A versatile BCS-based strategy has been introduced to design sparse conformal arrangements matching arbitrary far field patterns and fitting geometrical constraints. Within a probabilistic formulation, the sparsest array layout has been derived by exploiting a suitable generalization to conformal architectures of the Bayesian approach discussed in [27], [28]. The representative results from an extensive set of numerical experiments have proved that (*i*) the synthesis of arbitrarily shaped arrays (Section IV-A) comprising directive elements [(1)] is enabled; (*ii*) element saving ratios within the range $\nu \in [0.6, 0.9]$ can be yielded (Section IV) still accurately matching the reference pattern; (*iii*) constraints on the aperture (Section IV-B) and, unlike the $1D$ and $2D$ cases, on the minimum inter-element distance (Section IV-C) are effectively dealt with; (*iv*) despite the non-optimized nature of the considered software implementation, the proposed method always requires a reduced computational time to perform a conformal array synthesis ($\Delta t \leq 40$ [s]—Table I–III). Those results have been obtained thanks to the following main methodological contributions:

- the generalization of the guidelines in [27], [28] to the conformal structure;
- the introduction of the radiation pattern of the array elements within the synthesis procedure, which has never been integrated in CS-based sparse array synthesis techniques [24], [27], [28];
- the derivation of a suitable set of aperture and pattern sampling strategies to mitigate the higher ill-posedness of the transformation kernel of the conformal problem;
- the integration within the synthesis process of an *element merging* procedure for constraining the inter-element distance of the final layout without reducing the number of DOFs of the synthesis process.

Future works, outside the scope of the present paper, will be devoted to introduce mutual coupling models, which are of great importance for this kind of configurations, within the theoretical formulation of the $MT-BCS$ strategy in order to investigate its final limits and its effective applicability. Towards this end, the use of a mutual coupling matrix (for instance, computed through the induced EMF method [39] for dipole radiators) that pre-multiplies the radiation operator in (3) could be employed, therefore adapting the final solution (15) accordingly. Moreover, the exploitation of the same methodological approach to mask-constrained synthesis problems is at present under investigation.

Acknowledgment

The authors wish to thank Dr. S. Ji, Dr. Y. Xue, and Prof. L. Carin for sharing the BCS code online [37]. A. Massa wishes to thank A. Repetto, M. R. Repetto, R. G. Fumina, C. Pedrazzani, and L. Massa for their patience and support.

References

[1] R. J. Mailloux, "Chapter 22: Conformal and low-profile arrays," in *Antenna Engineering Handbook*, 4th ed. New York, NY, USA: McGraw-Hill, 2007.
[2] W. H. Kummer, "Preface to special issue on conformal antennas," *IEEE Trans. Antennas Propag.*, vol. 22, no. 1, pp. 1–3, Jan. 1974.
[3] A. Ludwig, "Curved array pattern synthesis," in *Proc. IEEE Antennas Propag. Soc. Int. Symp.*, Jun. 1985, vol. 23, pp. 123–126.
[4] I. Chiba, K. Hariu, S. Sato, and S. Mano, "A projection method providing low sidelobe pattern in conformal array antennas," in *Proc. IEEE Antennas Propag. Soc. Int. Symp.*, 1989, vol. 1, pp. 130–133.
[5] G. Mazzarella and G. Panariello, "Pattern synthesis of conformal arrays," in *IEEE Antennas Propag. Soc. Int. Symp.*, 1993, vol. 2, pp. 1054–1057.
[6] A. Tennant, "Numerical pattern synthesis of difference beams in conformal arrays," *Electron. Lett.*, vol. 31, no. 12, pp. 938–939, Jun. 1995.
[7] C. Dohmen, J. W. Odendaal, and J. Joubert, "Synthesis of conformal arrays with optimized polarization," *IEEE Trans. Antennas Propag.*, vol. 55, no. 10, pp. 2922–2925, Oct. 2007.
[8] O. M. Bucci, G. D'Elia, and G. Romito, "Power synthesis of conformal arrays by a generalised projection method," *IEE Proc. Microw. Antennas Propag.*, vol. 142, no. 6, pp. 467–471, Dec. 1995.
[9] O. M. Bucci and G. D'Elia, "Power synthesis of reconfigurable conformal arrays with phase-only control," *Proc. Inst. Elect. Eng. Microwave Antennas Propag.*, vol. 145, pp. 131–136, Feb. 1998.
[10] L. I. Vaskelainen, "Iterative least-squares synthesis methods for conformal array antennas with optimized polarization and frequency properties," *IEEE Trans. Antennas Propag.*, vol. 45, no. 7, pp. 1179–1185, Jul. 1997.
[11] L. I. Vaskelainen, "Phase synthesis of conformal array antennas," *IEEE Trans. Antennas Propag.*, vol. 48, no. 6, pp. 987–991, Jun. 2000.
[12] L. I. Vaskelainen, "Constrained least-squares optimization in conformal array antenna synthesis," *IEEE Trans. Antennas Propag.*, vol. 55, no. 3, pp. 859–867, Mar. 2007.
[13] E. C. Dufort, "Pattern synthesis based on adaptive array theory," *IEEE Trans. Antennas Propagat.*, vol. 37, no. 8, pp. 1011–1018, Aug. 1989.
[14] B. Fuchs, "Shaped beam synthesis of arbitrary arrays via linear programming," *IEEE Antennas Wireless Propag. Lett.*, vol. 9, pp. 481–484, 2010.
[15] J. A. Ferreira and F. Ares, "Pattern synthesis of conformal arrays by the simulated annealing technique," *Electron. Lett.*, vol. 33, no. 13, pp. 1187–1189, 1997.
[16] D. W. Boeringer and D. H. Werner, "Efficiency-constrained particle swarm optimization of a modified Bernstein polynomial for conformal array excitation amplitude synthesis," *IEEE Trans. Antennas Propag.*, vol. 53, no. 8, pp. 2662–2673, Aug. 2005.
[17] W. T. Li, S. F. Liu, X. W. Shi, and Y. Q. Hei, "Low-sidelobe pattern synthesis of spherical array using the hybrid genetic algorithm," *Microw. Opt. Technol. Lett.*, vol. 51, no. 6, pp. 1487–1491, Jun. 2009.
[18] W. T. Li, X. W. Shi, Y. Q. Hei, S. F. Liu, and J. Zhu, "A hybrid optimization algorithm and its application for conformal array pattern synthesis," *IEEE Trans. Antennas Propag.*, vol. 58, no. 10, pp. 3401–3406, Oct. 2010.
[19] J. O. Yang, Q. R. Yuan, F. Yang, H. J. Zhou, Z. P. Nie, and Z. Q. Zhao, "Synthesis of conformal phased array with improved NSGA-II algorithm," *IEEE Trans. Antennas Propag.*, vol. 57, no. 12, pp. 4006–4009, Dec. 2009.
[20] J. S. Sun, D. S. Goshi, and T. Itoh, "Optimization and modeling of sparse conformal retrodirective array," *IEEE Trans. Antennas Propag.*, vol. 58, no. 3, pp. 977–981, Mar. 2010.
[21] P. Rocca, M. Benedetti, M. Donelli, D. Franceschini, and A. Massa, "Evolutionary optimization as applied to inverse scattering problems," *Inverse Problems*, vol. 25, no. 12, pp. 1–41, Dec. 2009.

[22] R. L. Haupt, "Thinned arrays using genetic algorithms," *IEEE Trans. Antennas Propag.*, vol. 42, no. 7, pp. 993–999, Jul. 1994.
[23] P. Rocca, G. Oliveri, and A. Massa, "Differential evolution as applied to electromagnetics," *IEEE Antennas Propag. Magazine*, vol. 53, no. 1, pp. 38–49, Feb. 2011.
[24] G. Oliveri and A. Massa, "Bayesian compressive sampling for pattern synthesis with maximaly sparse non-uniform linear arrays," *IEEE Trans. Antennas Propag.*, vol. 59, no. 2, pp. 467–481, Feb. 2011.
[25] S. Ji, Y. Xue, and L. Carin, "Bayesian compressive sensing," *IEEE Trans. Signal Process.*, vol. 56, no. 6, pp. 2346–2356, Jun. 2008.
[26] M. E. Tipping, "Sparse Bayesian learning and the relevance vector machine," *J. Machine Learning Res.*, vol. 56, pp. 211–244, Jun. 2001.
[27] G. Oliveri, M. Carlin, and A. Massa, "Complex-weight sparse linear array synthesis by Bayesian compressive sampling," *IEEE Trans. Antennas Propag.*, vol. 60, no. 5, pp. 2309–2326, May 2012.
[28] F. Viani, G. Oliveri, and A. Massa, "Compressive sensing pattern matching techniques for synthesizing planar sparse arrays," *IEEE Trans. Antennas Propag.*, vol. 61, no. 9, pp. 4577–4587, Sept. 2013.
[29] G. Oliveri, P. Rocca, and A. Massa, "A Bayesian compressive sampling-based inversion for imaging sparse scatterers," *IEEE Trans. Geosci. Remote Sens.*, vol. 49, no. 10, pp. 3993–4006, Oct. 2011.
[30] L. Poli, G. Oliveri, and A. Massa, "Microwave imaging within the first-order Born approximation by means of the contrast-field Bayesian compressive sensing," *IEEE Trans. Antennas Propag.*, vol. 60, no. 6, pp. 2865–2879, Jun. 2012.
[31] G. Oliveri, L. Poli, P. Rocca, and A. Massa, "Bayesian compressive optical imaging within the Rytov approximation," *Opt. Lett.*, vol. 37, no. 10, pp. 1760–1762, 2012.
[32] G. Oliveri, P. Rocca, and A. Massa, "Reliable diagnosis of large linear arrays—Bayesian compressive sensing approach," *IEEE Trans. Antennas Propag.*, vol. 60, no. 10, pp. 4627–4636, Oct. 2012.
[33] R. G. Baraniuk, "Compressive sampling," *IEEE Signal Process. Mag.*, vol. 24, no. 4, pp. 118–124, Jul. 2007.
[34] E. J. Candes and T. Tao, "Decoding by linear programming," *IEEE Trans. Inf. Theory*, vol. 51, no. 12, pp. 4203–4215, Dec. 2005.
[35] S. Ji, D. Dunson, and L. Carin, "Multi-task compressive sampling," *IEEE Trans. Signal Process.*, vol. 57, no. 1, pp. 92–106, Jan. 2009.
[36] M. E. Tipping and A. C. Faul, "Fast marginal likelihood maximization for sparse Bayesian models," in *Proc. 9th Int. Workshop Artificial Intell. Stat.*, C. M. Bishop and B. G. Frey, Eds., 2003.
[37] S. Ji, Y. Xue, and L. Carin, *Bayesian Compressive Sensing Code,* [Online]. Available: http://people.ee.duke.edu/~lcarin/BCS.html
[38] B. P. Kumar and G. R. Branner, "Generalized analytical technique for the synthesis of unequally spaced arrays with linear, planar, cylindrical or spherical geometry," *IEEE Trans. Antennas Propag.*, vol. 53, no. 2, pp. 621–634, Feb. 2005.
[39] C. A. Balanis, *Antenna Theory: Analysis and Design*. New York, NY, USA: Wiley, 1997.

Giacomo Oliveri (M'07–SM'13) received the B.S. degree (*summa cum laude*) and M.S. (*summa cum laude*) degrees in telecommunications engineering and the Ph.D. degree in space sciences and engineering from the University of Genoa, Italy, in 2003, 2005, and 2009, respectively.

He is currently an Assistant Professor at the Department of Information Engineering and Computer Science, University of Trento, Italy, and a member of the ELEDIA Research Center. He is author/co-author of over 150 peer reviewed papers on international journals and conferences. He has been a visiting researcher at the University of Paris Sud, France, in 2012 and 2013. His research work is mainly focused on electromagnetic direct and inverse problems, system-by-design approaches, innovative metamaterials, and antenna array design and synthesis.

Ephrem T. Bekele received the B.Sc. degree in electrical engineering from Bahir Dar University, Bahir Dar, Ethiopia, in 2007. He received the M.Sc. degree in telecommunications engineering from University of Trento, Trento, Italy, in 2011. He is currently pursuing the Ph.D. degree from the ICT International Doctoral School of Trento, and conducting research in the ELEDIA Research Center.

He worked as an Assistant Lecturer in Bahir Dar University in 2007–2009. His main research interests are antenna arrays and electromagnetic inverse scattering.

Fabrizio Robol received the B.S. and the M.S. degree in telecommunication engineering from the University of Trento, Italy, in 2009 and 2011 respectively. He is a member of the ELEDIA Research Center where he is pursuing the Ph.D degree in the ICT International Doctoral School of Trento.

His research work is focused on wireless sensor network, electromagnetic propagation and antenna design.

Andrea Massa received the laurea degree in electronic engineering the Ph.D. degree in electronics and computer science from the University of Genoa, Genoa, Italy, in 1992 and 1996, respectively.

From 1997 to 1999 he was an Assistant Professor of Electromagnetic Fields at the Department of Biophysical and Electronic Engineering (University of Genoa) teaching the university course of Electromagnetic Fields 1. From 2001 to 2004, he was an Associate Professor at the University of Trento. Since 2005, he has been a Full Professor of Electromagnetic Fields at the University of Trento, where he currently teaches electromagnetic fields, inverse scattering techniques, antennas and wireless communications, and optimization techniques. He is the director of the ELEDIA Research Center at the University of Trento. Moreover, he is Adjunct Professor at Penn State University (USA), and Visiting Professor at the Missouri University of Science and Technology (USA), at the Nagasaki University (Japan), at the University of Paris Sud (France), and at the Kumamoto University (Kumamoto-Japan). His research work since 1992 has been principally on electromagnetic direct and inverse scattering, microwave imaging, optimization techniques, wave propagation in presence of nonlinear media, wireless communications and applications of electromagnetic fields to telecommunications, medicine and biology.

Prof. Massa is a member of the IEEE Society, of the PIERS Technical Committee, of the Inter-University Research Center for Interactions Between Electromagnetic Fields and Biological Systems (ICEmB), and he has served as Italian representative in the general assembly of the European Microwave Association (EuMA). He serves as an Associate Editor of the IEEE TRANSACTIONS ON ANTENNAS AND PROPAGATION.